Cell Proliferation

Cell Prolif., 2014, **47**, 347–355 doi: 10.1111/cpr.12110

Mathematical modelling of spatio-temporal cell dynamics in colonic crypts following irradiation

T. Murano*, Y. Kagawa† and S. Tsuneda*

**Department of Life Science and Medical Bioscience, Waseda University, Tokyo, Japan and †Institute for Nanoscience and Nanotechnology, Waseda University, Tokyo, Japan*

Received 14 March 2014; revision accepted 17 March 2014

Abstract

Objectives: Modelling the apoptotic process is essential for simulating and understanding tumour growth, as most tumour tissues carry mutations in apoptotic signalling pathways. Thus here, we have aimed to construct a mathematical model of colonic crypts that explicitly incorporates the apoptotic mechanism.

Methods: A murine colonic crypt was described as being a two-dimensional rectangular surface model. In this system, three types of cells with different proliferating and differentiating potentials migrate. Apoptosis was described as a process activated by irradiation that progresses in a stepwise manner. Parameter values in the model were determined to be consistent with experimental data for changes in the apoptotic cell ratio within murine transverse colonic crypts following irradiation.

Results: First, we constructed a model reproducing cell proliferation dynamics in normal murine colonic crypts; next, we applied the apoptotic mechanism to this model. As a result, we succeeded in simultaneous reproduction of both spatial and temporal changes in distribution of apoptotic cells in murine colonic crypts by determining parameter values in numerical simulations. Through this adjustment process, we were able to predict that stem cells and transit amplifying (TA) cells in each generation must react distinctly from each other, to apoptosis-inducing stimuli.

Conclusions: We constructed a mathematical model with which we could quantitatively describe cell proliferative and apoptotic dynamics in a murine colonic crypt. Using this model, we were able to make novel predictions that sensitivity to apoptosis-inducing stimuli is dependent on cell type.

Correspondence: S. Tsuneda, Department of Life Science and Medical Bioscience, Waseda University, Tokyo 162-8480 Japan. Tel.: +81 3 5369 7325; Fax: +81 3 3341 2684; E-mail: stsuneda@waseda.jp

Introduction

In homoeostasis, number of cells in living tissues is controlled by balance between cell proliferation and cell loss by processes that include apoptotic and living cell extrusion (1). Studies of such homoeostasis are essential for understanding mechanisms of tumour growth and for developing novel anti-cancer treatments. Thus, there have been many studies of homoeostasis of intestinal epithelial tissues, in which cells proliferate very frequently and migrate actively.

To quantitatively describe intestinal epithelial tissues as a dynamic system, dynamic parameters, such as cell-cycle duration and speed of cell migration, need to be estimated. In conventional experimental methods, these dynamic parameters have been estimated indirectly by the statistical figures of fixed tissue samples based on several hypotheses generated using cell dynamics (2). To estimate the parameters directly, development of *in vitro* culture systems for intestinal tissues is required. Recently, some research groups have succeeded in culturing a single intestinal crypt *in vitro* (3,4), where proliferating and migrating cells could be directly observed by microscopy.

As an alternative, mathematical modelling is a powerful method to understand dynamic systems behind experimental data. In earlier models, surface of the intestinal crypt has been characterized as a two-dimensional rigid lattice with rectangular cell layouts (5,6). Using this model, some cell dynamics have been described. However, this describes several unrealistic aspects inconsistent with real crypt dynamics; for example, migration of individual cells, as their movement would be restricted to discrete spatial steps. To resolve these

difficulties, a two-dimensional lattice-free model has been proposed (7). Here, individual cell shape was depicted to result from location of the centre of the cell, and boundaries between all neighbouring cell centres were described using Voronoi diagrams. A further similar model for describing cell shape has been constructed (8). In this model, the Wnt signalling network was implemented; cell-cycle and adhesion/repulsion forces between neighbouring cells are changed by distinct Wnt stimulation, which has been suggested in previous experimental results. Recently, a three-dimensional model for murine small intestinal crypts has been developed (9). In this model, Wnt and Notch signals determined cell differentiation. Our group has also constructed a mathematical model to describe processes of cell proliferation and differentiation in a human colonic crypt, and has succeeded in simulating several experimental results (10).

In most of these previous crypt models, apoptosis occurred only at the top of the crypt to maintain crypt cell number. In contrast, considering that most tumour tissues carry mutations in apoptotic signalling pathways, modelling of the apoptotic process is needed for simulating and understanding tumour growth. Thus, in this study, to simulate tumour tissue development, we sought to construct a mathematical model of colonic crypts in which apoptotic mechanisms are incorporated. To achieve this, we attempted to integrate mechanism of apoptosis into our previously constructed model to describe tumour growth in which apoptosis is disordered. To validate the model quantitatively, experimental data relating to apoptosis are needed. However, apoptosis is rarely detected in healthy crypts (11). Therefore, we used data for apoptotic dynamics induced by irradiation. Irradiation experiments were intensively performed in the 1970s to investigate the process of tissue regeneration (12). In these experiments, apoptotic index (AI), percentage of cells showing apoptotic bodies in tissue, was obtained as quantitative data. In the present study, we found the apoptotic mechanism to be consistent with AI data obtained in the irradiation experiments.

Methods

Modelling cell proliferation and migration in murine colonic crypts

A colonic crypt was modelled as a hollow cylindrical shape, whose development is described as a two-dimensional rectangular surface (Fig. 1a). On this surface, cells migrate and differentiate. The following three cell phenotypes were considered: stem, TA and differentiated cells.

Among these, only stem cells can self-replicate, and stem cell cycle time was defined as C_S. During the cell cycle, a cell doubles its size. That is, the cell radius r_t at time t is given by

$$r_t = \left(1 + \left(\sqrt{2} - 1\right)\frac{t}{C_S}\right) \times r_0 \tag{1}$$

where r_0 is the initial cell radius value. The rule for division of stem cells depends on their position. The region from the crypt bottom to height of b is defined as 'replication region of stem cells'. In this region, a stem cell divides symmetrically into two stem cells with a probability of P. Furthermore, a stem cell divides asymmetrically into one stem cell and one TA cell with a probability of $1 - P$. At the upper end of this region, a stem cell always divides symmetrically into two TA cells.

A TA cell produced by a stem cell divides symmetrically a limited number of times. In the g-th division, the TA cell differentiates into two differentiated cells; its cell cycle time is defined as C_{TA}. TA cell radius is also given by eqn (1). Differentiated cells never divide. Figure 1b summarizes cell proliferation and differentiation.

When a cell divides, its division axis, and centre positions of its daughter cells along division axis after division are determined (10). A dividing axis is determined as the axis passing through the centre of the dividing cell (mother cell) (x_M, y_M). Centres of daughter cells are determined as (x_{D1}, y_{D1}) and (x_{D2}, y_{D2}), respectively, where $x_{D1} = x_M + r_0\sin\theta$, $y_{D1} = y_M + r_0\cos\theta$, $x_{D2} = x_M - r_0\sin\theta$ and $y_{D2} = y_M - r_0\cos\theta$. θ is an angle randomly sampled from the range of $[-\pi, \pi]$ radian.

When daughter cells are generated by cell division, cells can overlap. To avoid overlaps, the 'shoving' algorithm, in which cells 'shove' each other to minimize overlapping area, is performed to arrange cell positions (10). In this algorithm, first, a cell (denoted by cell a) is chosen and its neighbouring cells (denoted by cells j; $j = 1, 2, \ldots, n_a$) are determined as those attached to the first chosen cell. Next, the following sums are calculated:

$$\delta x^{(a)} = \sum_{j=1}^{n_a} \frac{x^{(j)} - x^{(a)}}{d^{(j)}}\left[\left(R^{(j)} + R^{(a)}\right) - d^{(j)}\right], \tag{2}$$

$$\delta y^{(a)} = \sum_{j=1}^{n_a} \frac{y^{(j)} - y^{(a)}}{d^{(j)}}\left[\left(R^{(j)} + R^{(a)}\right) - d^{(j)}\right], \tag{3}$$

where

$$d^{(j)} = \sqrt{\left(x^{(j)} - x^{(a)}\right)^2 + \left(y^{(j)} - y^{(a)}\right)^2}$$

represents distance between centres of cells a and j, $R^{(a)}$ and $R^{(j)}$ represent radii of cells a and j, respectively, and

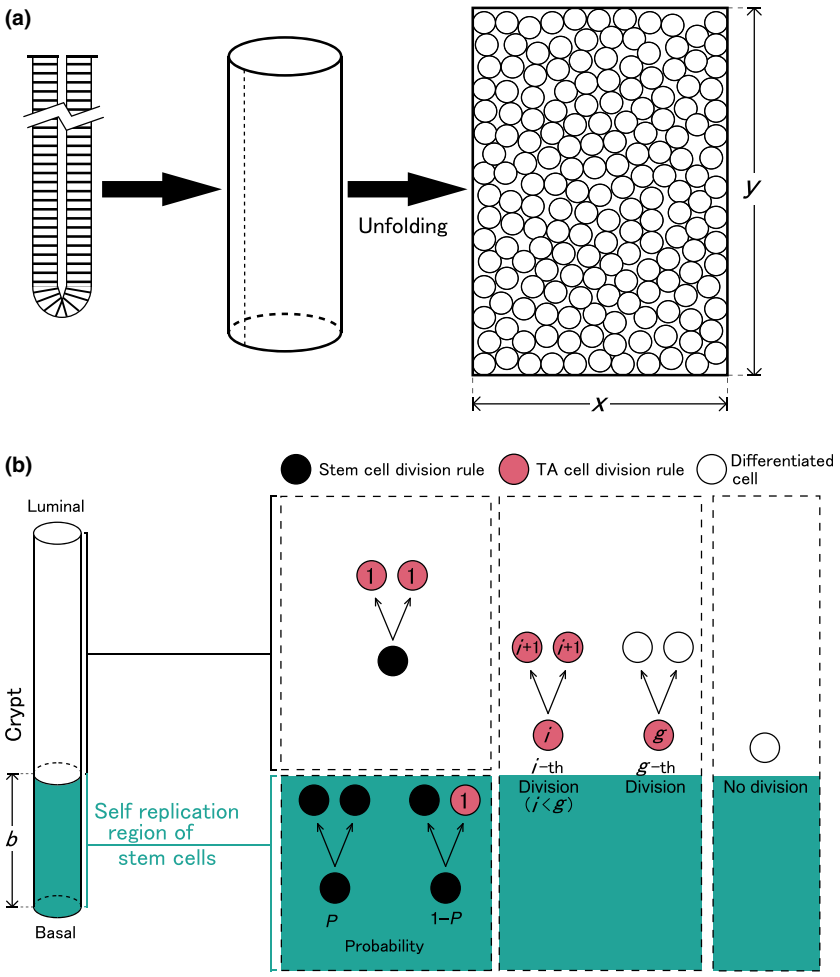

Figure 1. Model of murine colonic crypt. (a) Modelling of the crypt. A crypt is modelled as a cylindrical surface, which is unfolded to a two-dimensional surface. Cells are spatially arranged on this rectangular surface whose width and height are given by x and y, respectively. (b) Scenario of cell proliferation and differentiation. Two regions are considered in a crypt. Lower portion of the crypt, whose height is b, is defined as the self-replication region of stem cells. Within this region, a stem cell divides symmetrically and produces two stem cells with a probability P $(0 \leq P \leq 1)$. When it divides asymmetrically, it produces a stem cell and a first-generation transit amplifying (TA) cell with a probability $1 - P$. Outside this region, a stem cell divides symmetrically and produces two-first-generation TA cells. Regardless of the region, a TA cell divides symmetrically and differentiates after g-th divisions.

$(x^{(a)}, y^{(a)})$ and $(x^{(j)}, y^{(j)})$ represent positions of cells a and j in two-dimensional model space, respectively (10). Last, position of cell a is changed from $(x^{(a)}, y^{(a)})$ to $(x^{(a)} + \delta x^{(a)}, y^{(a)} + \delta y^{(a)})$. A set of these procedures is executed for all cells in the model, successively. In the present simulations, this procedure was repeated 1000 times for each shoving step.

As a result of the shoving algorithm, cells on average, move upwards. When cells arrive at the top of the crypt, they are removed from it. This removing process emulates the exfoliating process occurring at the top of real colonic crypts.

Calibrating parameters of cell proliferation and differentiation

To quantify cell proliferation in murine colonic crypts, many experiments using thymidine-analogues have been conducted. In the 1970s, tritiated thymidine ([^{3}H]dT) was injected into mice, and their large intestines (transverse colons) were dissected and fixed for autoradiographical analysis, where number of cells incorporating thymidine analogues was counted (13). In such experiments, labelling index (LI), defined as a ratio of labelled (thymidine analogues incorporated) cells, was given for each cell position in the crypt. We used such LI data, obtained experimentally in a previous study (13), for calibration of the model parameter values that determine cell dynamics in a crypt.

Calibration was executed by quantitatively comparing LI data obtained in the experiment with LI data calculated by model simulation, using a given parameter set. In the simulation, all S-phase cells at the time of thymidine analogue injection were labelled. One hour after labelling, we calculated ratios of labelled cells in each cell position along a vertical (that is, crypt–villus) axis of the crypt. As shown in Fig. S1, vertical lines were drawn on the crypt surface at intervals of 5 μm. Next, on each line, labelling status (labelled or non-labelled) of cells was recorded for each cell position,

defined as number of cells counted from the bottom, along the line. Last, LI was calculated as $n_i(\%)$ (i = 1, 2, . . .) (Fig. S1).

As the existing ratio for each cell type can fluctuate around the mean value with time, LI depends on time when the thymidine analogue was injected. Therefore, in the present simulations, the thymidine analogue was injected at three different time points after the number of cells of each species reaches a steady state. Three LI curves calculated for a series of three thymidine analogue injections were averaged and used for calibration of the model parameter values.

Modelling apoptosis in colonic crypts

To describe by a constructed model, cell behaviour in colonic crypts after irradiation, implementation of the apoptosis process was essential. When a cell executes apoptosis in living tissues, several signalling pathways are activated and various reactions occur sequentially (14,15). During apoptosis in colonic crypts, the reaction pathway shown in Fig. 2a is considered to progress in a stepwise manner. When cells are exposed to stresses such as hypoxia and irradiation, their DNA is damaged. When damage is too severe to be sustained, the cells initiate apoptosis. First, various apoptotic proteins such as BAX and BAK oligomerize on outer membranes of mitochondria, and these oligomers create pores. This is called mitochondrial outer membrane permeabilization and is irreversible. As a result, cytochrome *c* is released from inter-membrane spaces of the mitochondria into the cytoplasm, and downstream reactions are activated sequentially. Finally, caspase-3, the executor of apoptosis, is activated. Subsequently, this dismantles cells and causes cell death. Cell fragments – apoptotic bodies, are phagocytosed by macrophages and/or adjacent epithelial cells.

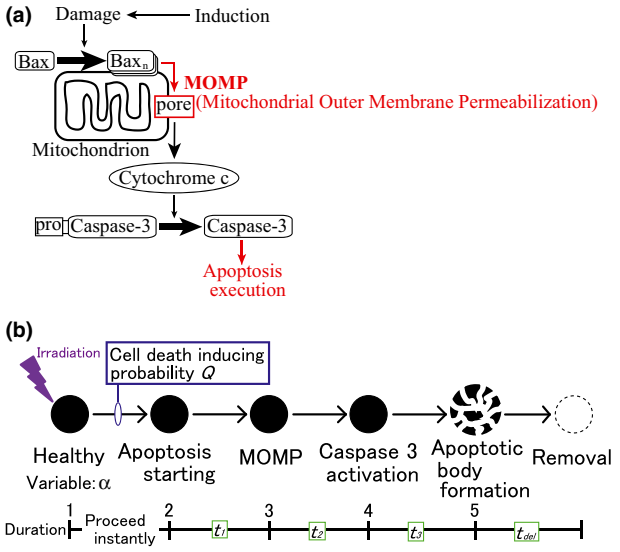

Figure 2. Modelling of the apoptotic process. (a) Schematic drawing of the apoptotic pathway, starting from DNA damage persisting after induction. This progresses in a stepwise manner. (b) Cells at each stage are assigned with a variable α. After irradiation, cells (α = 1) induce apoptosis with probability Q. Following this, the apoptotic process progresses sequentially with given time durations; between each stage these are assigned as t_1, t_2, t_3, and t_{del}.

As apoptosis progresses in a stepwise manner, it has been subdivided into five stages in the present model (Fig. 2b). An integer variable α was assigned to each cell to describe the stage of apoptotic progression. Figure 2b shows the relationship between value of α and corresponding apoptotic stage. In cells with α = 1, no apoptotic process is activated. When cells are irradiated, a subset of cells undergoes apoptosis as a result of DNA double-strand breaks, and the variable α is changed to 2. This change of α from 1 to 2 occurs stochastically with a probability of Q. Subsequent changes of α from 2 to 3, 3 to 4 and 4 to 5 occur as time elapses. Durations between states of α = 2, 3, 4 and 5 are defined as t_1, t_2 and t_3, respectively. Cells with α = 5 are removed from the model crypt after duration t_{del}.

Calculation of apoptosis index

In previously reported experimental studies, AI has been measured along the cell position for a given time, to estimate apoptotic frequency within the crypt. AI at cell position i was defined as proportion of apoptotic cells found at i. AI curve provided in the literature (11) has been plotted in Fig. 5a (closed circles). In the same study (11), time courses of AI after irradiation, defined as ratio of apoptotic cells in a whole crypt, were also provided (closed circles in Fig. 5b). In the present model, cells with α = 4 or 5, corresponding to cells in which caspase-3 was activated, were considered to be apoptotic cells. Using results the simulation, we calculated AIs along the cell positions at specified times corresponding to the experiments. We also calculated time course of AI in the crypt as a whole after apoptosis induced by irradiation. Finally, we compared these values with the corresponding experimental data (11).

In the simulation, a model crypt was stimulated by irradiation at a given time point after number of cells of each phenotype reached a steady state. For each given parameter set, three simulation results with different stimulation time points were averaged and the AI curve was obtained. We searched for parameter values in which the simulation results were consistent with the experimental data (11).

Assessment of fitness to experimental data

To quantify similarity of simulation results to experimental data (LI and AI), the value of D was used (10). D is defined as the absolute difference between simulation results and experimental data, averaged over cell positions i:

$$D = \sum_{i=1}^{M} \Big| [\text{simulation results (LI or AI)}] - [\text{experimental data (LI or AI)}] \Big| / M$$

where M is number of plots. To calibrate model parameters, we searched for the parameter set minimizing D by changing values of the parameters.

Results

Cell proliferation and migration

Initial cell radius, and width and height of the model crypt (r_0, x and y, respectively) were determined to be consistent with previous reports measuring size of colonic crypts (Table 1) (13,16). Following the method described above, model parameters relating to cell dynamics in the crypt were determined to be consistent with the experimental data. As shown in Fig. 3, the LI curve obtained with simulation results of the model was well adjusted to the experimental data (13) using the parameter values shown in Table 1.

To investigate sensitivity of changing each model parameter on the resultant LI curve, we changed one of the five dynamic model parameters b, g, C_S, C_{TA}, or P while the others remained fixed. Results of sensitivity analysis are shown in Fig. S2a–e. When height of the self-replication region of stem cells b was increased, LI values also increased globally (Fig. S2a). When maximum division count of TA cells g was increased, LI values in the upper part of the crypt increased dramatically (see Fig. S2b). When stem cell cycle C_S was reduced, as shown in Fig. S2c, LI values increased in lower and also in upper portions of the crypt. When TA cell cycle C_{TA} was changed, as shown in Fig. S2d, LI curve characteristically changed in response to C_{TA}. When C_{TA} decreased, LI values at the crypt base increased, while those in the upper portion reduced simultaneously. When probability of symmetrical division of stem cell P was changed, as shown in Fig. S2e, LI values slightly increased with increasing P.

Table 1. Parameters of the murine colonic crypt model

Parameter	Symbol	Value
Crypt architecture		
Crypt height	y	460 μm
Crypt circumference	x	230 μm
Number of cells in a crypt		684 cells
Initial cell radius	r_0	5 μm
Cell proliferation and differentiation		
Self-replication region of stem cell	b	20 μm
Stem-cell cycle	C_S	35 h (±5 h)
TA cell cycle	C_{TA}	25 h (±5 h)
Maximum division count	g	3
Probability of symmetrical division of stem cells	P	0.9
Apoptotic process		
Apoptosis-inducing probability of stem cell	Q_S	20%
Apoptosis-inducing probability of TA cell (first generation)	Q_{TA1}	70%
Apoptosis-inducing probability of TA cell (second generation)	Q_{TA2}	17.5%
Apoptosis-inducing probability of TA cell (third generation)	Q_{TA3}	0%
Minimum time duration between apoptosis starting and MOMP	t_{1Min}	80 min
Maximum time duration between apoptosis starting and MOMP	t_{1Max}	235 min
Time duration between apoptotic body formation and removal	t_{del}	40 min

TA, transit amplifying; MOMP, mitochondrial outer membrane permeabilization.

Apoptosis in murine colonic crypts

Apoptosis is considered to be induced through a system that monitors damage in cells at each cell cycle check-

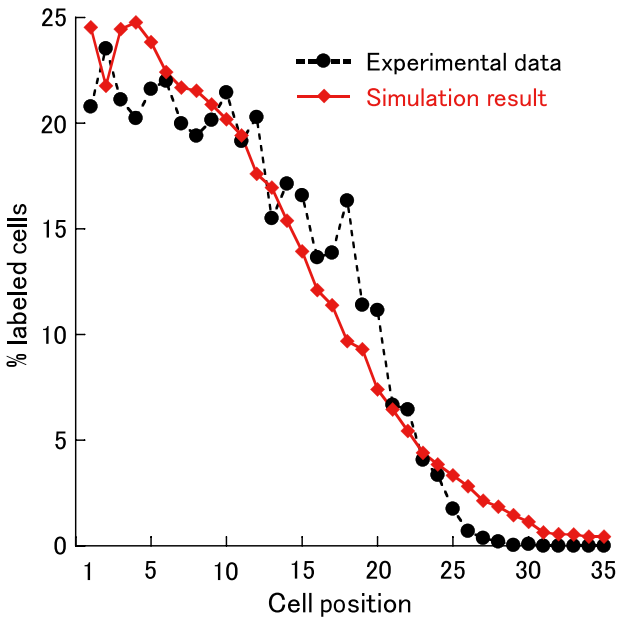

Figure 3. Labelling indices plotted against cell position. Simulation results (red closed diamonds and solid curve) were in good agreement with the experimental data (black closed circles and dashed curve) (13). To obtain these results, parameter values shown in Table 1 were used.

point. Based on this consideration, in our model, we assumed that only dividing cells could execute apoptosis, and thus apoptosis not occurring in differentiated cells. In addition, we assumed that cell dynamics was not affected/hardly affected by damage caused by irradiation. Therefore, in the following simulations, we used the parameter values shown in Table 1.

First, we simulated cases in which apoptosis occurred in specific cell phenotypes. In cases where apoptosis occurred only in stem cells, it occurred only at bases of crypts (in cell positions 1–5); thus AIs could not be adjusted to the experimental data. If apoptosis occurred only in TA cells, it occurred at any region along the various cell positions, and AIs in middles of crypts were much larger than those in lower regions. Again, AIs could not be adjusted to the experimental data. These results indicate that apoptosis occurred in both stem cells and TA cells.

Therefore, we simulated a situation in which apoptosis occurred in both cell phenotypes. Although numbers of parameters to be calibrated was increased from one to two, that is, probability of inducing apoptosis following irradiation to stem cells and TA cells (Q_S and Q_{TA}, respectively), we could not adjust the resultant AI curve to the experimental data by any combination of Q_S and Q_{TA} values. As we noticed that apoptotic cells disappeared in cell positions higher than 15 in the experimental data, we investigated distribution of stem and TA cells in each generation along the cell positions (Fig. 4). Here, we classified TA cells into first, second and third generations with number of cell divisions following differentiation to a TA cell. In this figure, a dominant phenotype residing at a given cell position gradually changed from a stem cell to a differentiated cell as the cell position was increased.

By defining the parameter values of Q_{TA} independently for each generation of TA cells, we could adjust the resultant AI curve to the experimental data (Fig. 5a). In this case, apoptosis occurred only in stem cells and first and second generation of TA cells. Only this case, could simulation results be fitted to the experimental data. Values of apoptotic parameters, Q, t_1, t_2, t_3, and t_{del} for each cell phenotype used in the simulation are summarized in Table 1.

To obtain these parameter values, two assumptions on values of t_1, t_2, t_3 and t_{del} were made. In the first, values of t_1, t_2, t_3 and t_{del} did not depend on cell phenotype, that is the same parameter values were used in stem cell and TA cells, in all generations. In the second assumption, values of t_2 and t_3 were determined by the value of t_1. To calculate t_2 and t_3, relative ratio between

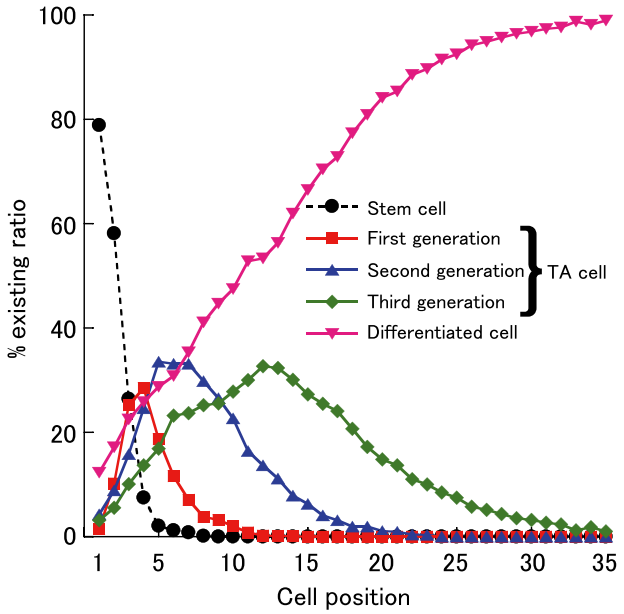

Figure 4. Existing ratio of each cell type. Existing ratios of stem (black circles), transit amplifying (TA) (first generation, red squares), TA (second generation, blue triangles), TA (third generation, green diamonds), and differentiated cells (pink inverted triangles) were plotted against cell position. To obtain these results, the parameter values shown in Table 1 were used.

t_1, t_2, and t_3, which had been obtained experimentally in a study using HeLa cells (17), was used. To be specific, t_2 and t_3 were estimated by, $t_2 = (8.76/65.88)\ t_1$ and $t_3 = (25.36/65.88)\ t_1$, respectively.

At first, simulations were performed with a given set of values for durations t_1, t_2, t_3. As there was clearly no apoptosis until time $t_1 + t_2$, under these conditions, it could not match the experimental data. Therefore, these time durations should be determined randomly from the assigned range. In the simulation, instead of calibrating values of t_1, its maximum value, t_{1Max}, and its minimum value, t_{1Min}, were calibrated as fitting parameters. Using t_{1Max} and t_{1Min}, maximum and minimum values of t_2 and t_3 were calculated by $t_{2Max} = (8.76/65.88)\ t_{1Max}$, $t_{2Min} = (8.76/65.88)\ t_{1Min}$, $t_{3Max} = (25.36/65.88)\ t_{1Max}$ and $t_{3Min} = (25.36/65.88)\ t_{1Min}$, respectively. Values of durations, t_1, t_2 and t_3, were sampled randomly from the corresponding ranges $[t_{1Min}, t_{1Max}]$, $[t_{2Min}, t_{2Max}]$ and $[t_{3Min}, t_{3Max}]$ by using uniform distribution. Furthermore, value of t_{del} was determined to be 40 min, as a result of simulations using various values of t_{del} (Fig. S3). Taken together, when parameter values were given by values shown in Table 1, simulation results [shown in Fig. 5 (closed diamonds)] could be fitted to the experimental data.

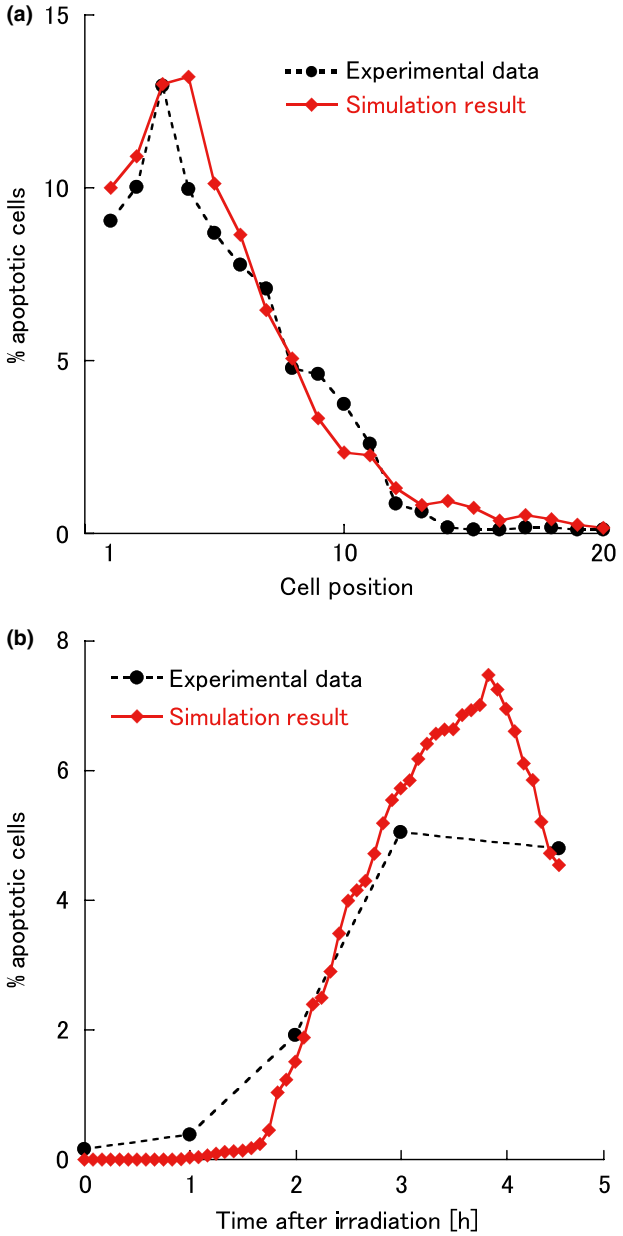

Figure 5. Spatial and temporal changes of apoptotic indices. (a) Apoptotic indices plotted against cell position (4.5 h after irradiation). (b) Apoptotic indices plotted against time after irradiation. These simulation results (red closed diamonds) were in good agreement with the experimental data (11) (black closed circles). Parameter values shown in Table 1 were used for the simulations.

Discussion

Model parameter values related to cell proliferation and differentiation

As a result of the simulations, average stem cell cycle C_S and average TA cell cycle C_{TA} were estimated to be 35 and 25 h, respectively. According to previous reports, cell cycle duration of cells located from the base to middle to upper portions of the crypt was in the order of 36 h (18) and 20 h (13,18,19), respectively. Considering that intestinal stem cells reside in the bases of crypts (20), estimated values of C_S and C_{TA} are consistent with these previously reported data. In a more recent report, crypt base columnar cells, which are considered to coincide with stem cells in the small intestinal crypt, have mean cell cycle duration of 28.5 h (21). In a further recent report, cells at the base of the crypt expressing Lgr5, an intestinal stem-cell marker, were shown to have a mean cell cycle of 21.5 h (22). Considering that the stem cell cycle in small intestinal crypts is shorter than that in colonic crypts (18), values of C_S and C_{TA} estimated in this study are very close to these published data.

Here, the probability of symmetrical division of stem cells, P, was estimated to be 0.9. This value was lower than 1, likely to be because stem cells sometimes divide asymmetrically in crypt bases. This prediction is consistent with a previous report that stem cells divide asymmetrically in mice and human colonic crypts (23).

The height of the self-replication region of stem cells, b, was estimated to be 20 μm, implying that stem cells mainly reside in cell positions 1–2. This is consistent with the observation that stem cells reside at bases of colonic crypts (24,25).

Model parameter values related to apoptosis

As shown in Table 1, apoptosis-inducing probability Q in TA cells of the first generation (assigned as Q_{TA1}) was predicted to be larger than that of stem cells (Q_S) or second-generation TA cells (Q_{TA2}).

Localization of suppressors of apoptosis is one of the possible reasons why Q_S was smaller than Q_{TA1}. Expression of Bcl-2, a suppressor of apoptosis, has been reported to be confined to the base of the colonic crypt (26), where the stem cells expressing Lgr5 reside (25). Moreover, it was also reported that levels of both spontaneous and induced apoptosis in Bcl-2-null mice rose significantly and selectively at the bases of crypts, in comparison to crypts from wild-type mice (26,27).

Probability Q was reduced when generation of TA cells was increased (Table 1). We presumed this to be a mechanism to efficiently maintain healthy tissue by removing relatively long-lived cells with persistent DNA damage, only. To the best of our knowledge, molecular evidence for this mechanism is lacking. We hope that this evidence will be revealed in future studies.

Relationship with other existing models

In this paper, we show that we have constructed a computational model for simulating apoptotic dynamics in murine colonic crypts. While other existing crypt models describe intestinal cell dynamics in normal crypts under a steady state (5–10,20), our present model focuses on transient processes after irradiation, and has succeeded in describing AI data obtained from previously performed quantitative experimental studies.

Several models published recently, introduced signalling pathways relating to growth, differentiation, proliferation and self-replication such as Wnt, Notch and BMP (8,9,28). On the other hand, a model using a simple scenario for the mechanism of cell proliferation and differentiation has been able to describe satisfactorily cell dynamics in human colonic crypts (10). Because the present model focused on apoptotic dynamics, a simple scenario for proliferation and differentiation was used. If necessary, it is possible to incorporate more signalling pathways into our model.

Calibration methods

In our model, we calibrated parameter values to obtain reasonable simulation results by repeating simulations using various parameter values. However, there are more rigorous methods to calibrate model parameters. For example, a method using approximate Bayesian computation has been proposed. In previous studies, this method has been used for parameter estimation of a model describing DNA methylation pattern dynamics (29,30). In principle, such a method can also be applied to the current crypt model. However, this application seems unrealistic at present as the computational load is too heavy. Thus, developing a novel strategy to apply such sophisticated methods to calibrate parameter values of complex computational models including ours developed in this paper, is expected.

In conclusion, in this study we developed a computational model of cell dynamics in a murine colonic crypt, with which we can quantitatively calculate spatial distributions of proliferative and apoptotic cells, within a crypt. We calibrated model parameter values to be consistent with previously reported experimental data, and found that parameter values related to the apoptotic process were dependent on the cell phenotype; this will shortly be validated experimentally.

Acknowledgement

This research was partially supported by a Waseda University Grant for Special Research Projects (Project number 2013A-312).

References

1 Eisenhoffer GT, Loftus PD, Yoshigi M, Otsuna H, Chien CB, Morcos PA *et al.* (2012) Crowding induces live cell extrusion to maintain homeostatic cell numbers in epithelia. *Nature* **484**, 546–549.
2 Meinzer HP, Sandblad B (1985) A simulation model for studies of intestine cell dynamics. *Comput. Methods Programs Biomed.* **21**, 89–98.
3 Sato T, Vries RG, Snippert HJ, van de Wetering M, Barker N, Stange DE *et al.* (2009) Single Lgr5 stem cells build crypt-villus structures in vitro without a mesenchymal niche. *Nature* **459**, 262–265.
4 Ootani A, Li X, Sangiorgi E, Ho QT, Ueno H, Toda S *et al.* (2009) Sustained in vitro intestinal epithelial culture within a Wnt-dependent stem cell niche. *Nat. Med.* **15**, 701–706.
5 Loeffler M, Stein R, Wichmann HE, Potten CS, Kaur P, Chwalinski S (1986) Intestinal cell proliferation. I. A comprehensive model of steady-state proliferation in the crypt. *Cell Tissue Kinet.* **19**, 627–645.
6 Loeffler M, Potten CS, Paulus U, Glatzer J, Chwalinski S (1988) Intestinal crypt proliferation. II. Computer modeling of mitotic index data provides further evidence for lateral and vertical cell migration in the absence of mitotic activity. *Cell Tissue Kinet.* **21**, 247–258.
7 Meineke FA, Potten CS, Loeffler M (2001) Cell migration and organization in the intestinal crypt using a lattice-free model. *Cell Prolif.* **34**, 253–266.
8 van Leeuwen IMM, Mirams GR, Walter A, Fletcher A, Murray P, Osborne J *et al.* (2009) An integrative computational model for intestinal tissue renewal. *Cell Prolif.* **42**, 617–636.
9 Buske P, Galle J, Barker N, Aust G, Clevers H, Loeffler M (2011) A comprehensive model of the spatio-temporal stem cell and tissue organisation in the intestinal crypt. *PLoS Comput. Biol.* **7**, e1001045.
10 Kagawa Y, Horita N, Taniguchi H, Tsuneda S (2014) Modeling of stem cell dynamics in human colonic crypts in silico. *J. Gastroenterol.* **49**, 263–269.
11 Marshman E, Ottewell PD, Potten CS, Watson AJM (2001) Caspase activation during spontaneous and radiation-induced apoptosis in the murine intestine. *J. Pathol.* **195**, 285–292.
12 Hendry JH, Potten CS (1974) Cryptogenic cells and proliferative cells in intestinal epithelium. *Int. J. Radiat. Biol.* **25**, 583–588.
13 Sunter JP, Appleton DR, de Rodriguez MSB, Wright NA, Watson AJ (1979) A comparison of cell proliferation at different sites within the large bowel of the mouse. *J. Anat.* **129**, 433–442.
14 Spencer SL, Sorger PK (2011) Measuring and modeling apoptosis in single cells. *Cell* **144**, 926–939.
15 Weinberg RA (2007) The Biology of Cancer, pp. 307–356. New York: Garland Science.
16 Potten CS, Kellett M, Roberts SA, Rew DA, Wilson GD (1992) Measurement of in vivo proliferation in human colorectal mucosa using bromodeoxyuridine. *Gut* **33**, 71–78.
17 Goldstein JC, Waterhouse NJ, Juin P, Evan GI, Green DR (2000) The coordinate release of cytochrome c during apoptosis is rapid, complete and kinetically invariant. *Nat. Cell Biol.* **2**, 156–162.
18 Potten CS, Li YQ, O'Connor PJ, Winton DJ (1992) A possible explanation for the differential cancer incidence in the intestine, based on distribution of the cytotoxic effects of carcinogens in the murine large bowel. *Carcinogenesis* **13**, 2305–2312.
19 Potten CS (1986) Cell cycles in cell hierarchies. *Int. J. Radiat. Biol.* **49**, 257–278.
20 Potten CS (1998) Stem cells in gastrointestinal epithelium: numbers, characteristics and death. *Philos. Trans. R. Soc. Lond. B Biol. Sci.* **353**, 821–830.

21 Escobar M, Nicolas P, Sangar F, Laurent-Chabalier S, Clair P, Joubert D *et al.* (2011) Intestinal epithelial stem cells do not protect their genome by asymmetric chromosome segregation. *Nat. Commun.* **2**, 258.
22 Schepers AG, Vries R, van den Born M, van de Wetering M, Clevers H (2011) Lgr5 intestinal stem cells have high telomerase activity and randomly segregate their chromosomes. *EMBO J.* **30**, 1104–1109.
23 Quyn AJ, Appleton PL, Carey FA, Steele RJC, Barker N, Clevers H *et al.* (2010) Spindle orientation bias in gut epithelial stem cell compartments is lost in precancerous tissue. *Cell Stem Cell* **6**, 175–181.
24 Potten CS (1992) The significance of spontaneous and induced apoptosis in the gastrointestinal tract of mice. *Cancer Metastasis Rev.* **11**, 179–195.
25 Barker N, van Es JH, Kuipers J, Kujala P, van den Born M, Cozijnsen M *et al.* (2007) Identification of stem cells in small intestine and colon by marker gene Lgr5. *Nature* **449**, 1003–1007.
26 Merrit AJ, Potten CS, Watson AJ, Loh DY, Nakayama K, Nakayama K *et al.* (1995) Differential expression of bcl-2 in intestinal epithelia: correlation with attenuation of apoptosis in colonic crypts and the incidence of colonic neoplasia. *J. Cell Sci.* **108**, 2261–2271.
27 Pritchard DM, Potten CS, Korsmeyer SJ, Roberts S, Hickman JA (1999) Damage-induced apoptosis in intestinal epithelia from bcl-2-null and bax-null mice: investigations of the mechanistic determinants of epithelial apoptosis in vivo. *Oncogene* **18**, 7287–7293.
28 Zhang L, Lander AD, Nie Q (2012) A reaction-diffusion mechanism influences cell lineage progression as a basis for formation, regeneration, and stability of intestinal crypts. *BMC Syst. Biol.* **6**, 93.
29 Bonello N, Sampson J, Burn J, Wilson IJ, McGrown G, Margison GP *et al.* (2013) Bayesian inference supports a location and neighbour-dependent model of DNA methylation propagation at the MGMT gene promoter in lung tumours. *J. Theor. Biol.* **336**, 87–95.
30 Walters K (2012) Parameter estimation for an immortal model of colonic stem cell division using approximate Bayesian computation. *J. Theor. Biol.* **306**, 104–114.

Supporting Information

Additional Supporting Information may be found in the online version of this article:

Fig. S1 Illustration describing formation of a labelling index (LI) curve.

Fig. S2 Sensitivity analysis of model parameters.

Fig. S3 Sensitivity analysis of parameter t_{del}.